Domain microstructures and ferroelectric phase transition in $Pb_{0.35}Sr_{0.65}TiO_3$ films studied by second harmonic generation in reflection geometry

S. W. Liu,[a] S. Jolly,[b] and Min Xiao[c]
Department of Physics, University of Arkansas, Fayetteville, Arkansas 72701

Z. Yuan, J. Liu, and C. L. Chen
Department of Physics and Astronomy, University of Texas at San Antonio, San Antonio, Texas 78249, Texas Center for Superconductivity, University of Houston, Houston, Texas 77204, and Department of Physics, University of Houston, Houston, Texas 77204

Wenkai Zhu
Department of Physics, University of Houston, Houston, Texas 77204

(Received 18 October 2006; accepted 25 March 2007; published online 31 May 2007)

Second harmonic generation (SHG) measurements were performed in the reflection geometry using the femtosecond Ti:sapphire laser at the wavelength of 810 nm for $Pb_{0.35}Sr_{0.65}TiO_3$ films, which were epitaxially deposited on (001) MgO substrates by pulsed laser ablation under different oxygen pressures. We formulated the procedures to measure the ratios of the compensated fractions of both *c* domains and in-plane domains and the ratios of the components of the nonlinear susceptibility tensor under only a non-normal incidence of the fundamental beam. We applied this technique to characterize the domain microstructures of the $Pb_{0.35}Sr_{0.65}TiO_3$ films at three typical temperatures (78, 150, and 300 K) and found these films to exhibit a larger compensated fraction of *c* domains. The ratios of the components of the nonlinear susceptibility tensor were calculated to be relatively constant regardless of the temperature and the oxygen pressure. On the other hand, their SHG intensities were found to increase as the oxygen pressure goes lower, which is attributed to the higher density of the oxygen vacancies in the films. These films also exhibit the diffuselike phase transition in a very wide temperature range, which is attributed to the structural inhomogeneity and the nonuniform distribution of Pb^{2+} and Sr^{2+} in the $Pb_{0.35}Sr_{0.65}TiO_3$ films. © *2007 American Institute of Physics*. [DOI: 10.1063/1.2735406]

I. INTRODUCTION

Thin films of ferroelectric lead strontium titanate $(Pb,Sr)TiO_3$ (PST) have recently been regarded as an important candidate for applications in various tunable microwave devices (for example, phase shifter and high-Q resonators)[1,2] and also have the potential applications in the high-density dynamic random access memories (DRAMs). They exhibit bistable polarization states, high relative dielectric constant (ε_r) values, and also tunable ε_r by applying an electric field. Both applications are related to the polarization states of the ferroelectric films. In the case of the tunable microwave device, an in-plane bias field is usually applied to the coplanar electrodes on the top of the films to tune laterally the microwave dielectric constants, where the tunability is obviously dependent on the behaviors of the in-plane domains (a/b domains). In the case of the DRAM, a normal electric field can reverse the orientation of the out-of-plane domains (*c* domains) in the ferroelectric film. The efficiency and speed of DRAM depend on the fraction of *c* domains and their dynamics.[3]

On the other hand, ferroelectric thin films have received much attention for fabricating novel functional devices for optical applications. The typical perovskite ferroelectric materials have excellent linear optical properties such as a wide energy band gap (>3 eV), low absorption coefficient, and high refraction index (>2.0). Also, they often exhibit the large nonlinear responses to the optical electromagnetic wave such as electro-optic (E-O) effect, nonlinear optical absorption and refraction, and second harmonic generation (SHG), etc. Especially, the SHG process may be used as a highly sensitive probe to study the domain structures of the ferroelectric films because the efficiency of SHG is highly dependent on both the domains' structural symmetry and their orientations. Since $(Pb,Sr)TiO_3$ films are the materials which can only be epitaxially grown recently, their optical characterizations are basically absent. Our manuscript systematically studied their linear and second-order optical properties that are basis for their potential applications in optical devices.

Several groups (such as Gopalan and Raj [4] Barad *et al.*,[5] and Mishina *et al.*[3]) have investigated the domain structures of the ferroelectric $KNbO_3$, $Bi_4Ti_3O_{12}$, and $(Ba,Sr)TiO_3$ films, etc., by coherent and incoherent optical SHGs in the transmission geometry. However, the *c* domains do not contribute to SHG under the normal incidence in the transmission geometry. To probe the *c* domains, additional measurements under the non-normal incidence have to be performed. Mishina *et al.*[3] investigated the *c* domains of the $(Ba,Sr)TiO_3$ film under the non-normal incidence in the

[a]Electronic mail: sxl03@uark.edu
[b]Permanent address: School of Electrical and Computer Engineering and School of Physics, Georgia Institute of Technology, Atlanta, GA 30332.
[c]Electronic mail: mxiao@uark.edu

transmission geometry. However, their two-step procedures demand an initial normal incidence. Also, the reflection measurements have the advantage to avoid the disturbing effects from the substrate. It is especially important for measuring the film deposited on an opaque substrate, where the transmission configuration or the initial normal incidence in reflection configuration is very difficult and even impossible.

The linear and nonlinear optical properties of the PST films have not been reported in spite of their technical importance. In this paper, we deposited the $Pb_{0.35}Sr_{0.65}TiO_3$ thin films on (001) MgO substrates under different oxygen pressures. Their refraction indices and optical propagation modes were measured. The SHG was also measured in a temperature range from 78 to 320 K. The efficiency of SHG of the as-grown PST films was found to be highly dependent on the oxygen pressure. We also show how to probe the ratios of the three components of the nonlinear susceptibility tensor and the ratios of the compensated domain fractions in these films by SHG under only a non-normal incidence in the reflection geometry.

II. FILM EPITAXY AND STRUCTURE CHARACTERIZATION

The epitaxial $Pb_{0.35}Sr_{0.65}TiO_3$ thin films were grown on (001) MgO substrates by using pulsed laser ablation by a KrF excimer laser with a wavelength of 248 nm. To avoid the lead deficiency during the film growth, a high-density $(Pb,Sr)TiO_3$ ceramic target with the nominal Pb/Sr ratio of 35:65 plus 20 at. % excess Pb was adopted. The MgO substrates were rigorously treated to avoid the surface moisture. Five PST films were deposited on MgO substrates at the temperature of 820 °C under the different oxygen pressures (50, 150, 250, 350, and 450 mTorr). The samples were then postannealed under 1 atm of oxygen for 20 min before they were cooled down slowly. X-ray θ–2θ scans indicate that all five samples have the pure (00*l*) peaks. The θ rocking scans of these five samples show the full width at half maximum (FWHM) for the PST (002) peak is in the range of 0.40°–080° Figure 1 shows typical diffraction patterns of θ–2θ scans and θ rocking scan (as shown in the inset) for the film deposited under 50 mTorr of oxygen. Microstructure studies from electron microscopy indicate that the as-grown PST films have the epitaxial orientation relationship of PST(001)[100]‖MgO(001)[100]. The details of the optimal deposition conditions and structural characterizations for the PST thin films on (001) MgO substrates were described in Ref. 2.

III. LINEAR OPTICAL PROPERTIES

The refraction indices are required to calculate the various Fresnel factors. As will be discussed in Sec. IV B, these Fresnel factors are essential to analyze the SHG data measured under the non-normal incidence. The refraction indices of the PST films and MgO substrate, and also the propagation modes, were measured using the Metricon prism coupler with Rutile prism at the wavelengths of 532, 632.8, 708, 770, 820, and 840 nm. The light sources for these measurements are a green diode laser (532 nm), a He–Ne laser (632.8 nm),

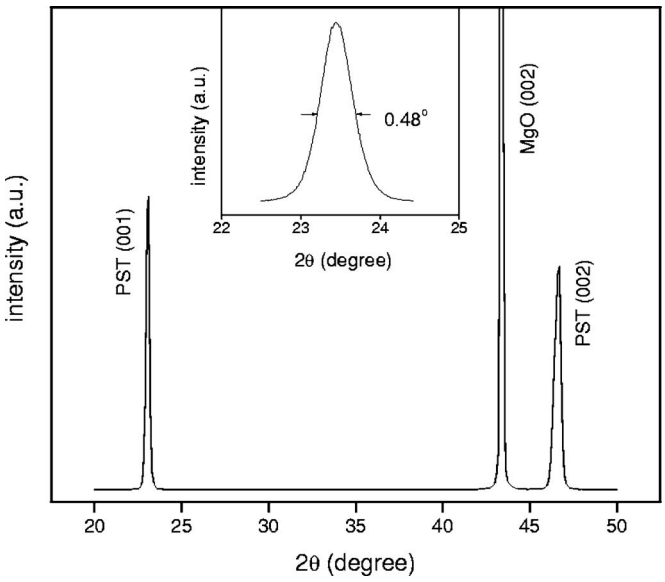

FIG. 1. X-ray diffraction patterns for the PST film deposited on a (001) MgO substrate under the oxygen pressure of 50 mTorr. θ–2θ scans show only (00*l*) reflections of the PST film, indicating the film is *c* axis oriented. The inset is a θ rocking curve measurement from the (002) PST reflection with the FWHM value of about 0.48°.

and a Ti:sapphire laser (708, 770, 820, and 840 nm), respectively. All refraction indices of the five PST films were calculated based on the observed angles for TE propagation modes, while the refraction index of MgO was calculated by locating the corresponding total reflection angle in a separate measurement for the bare MgO substrate. The refraction indices versus wavelengths for both PST and MgO were fitted via the following Cauchy function:

$$n = a + b/\lambda^2 + c/\lambda^4, \tag{1}$$

where n is the refraction index, λ is the wavelength (nanometer) and a, b, and c are the fitting parameters. These fits can then be used to obtain the indices at the fundamental wavelength (810 nm), and with less accuracy, to extrapolate to obtain index values at the SH wavelength (405 nm). Figure 2 shows a typical Cauchy fit for the film deposited under 50 mTorr. The inset shows a trend that the indices of the PST films at both 405 nm (open circle) and 810 nm (filled circle) decrease as the oxygen pressure goes higher because the lower oxygen pressure leads to a shrink of unit cell and thus a denser film. The refraction indices at low temperature were roughly estimated by considering the thermal coefficients of a typical perovskite and MgO crystal [roughly estimated as $(-8 \text{ and } -6)\times 10^{-5}\ K^{-1}$ for PST and $(1.3 \text{ and } 1.9)\times 10^{-5}\ K^{-1}$ for MgO at the fundamental and SH wavelengths, respectively[6]].

IV. SECOND HARMONIC GENERATION MEASUREMENTS

A. Experimental device and procedure

The experimental setup is shown in Fig. 3. The SH radiation is generated by a mode-locked Ti:sapphire laser with a high repetition rate of 82 MHz at the wavelength of 810 nm, which has a temporal width of about 300 fs. This

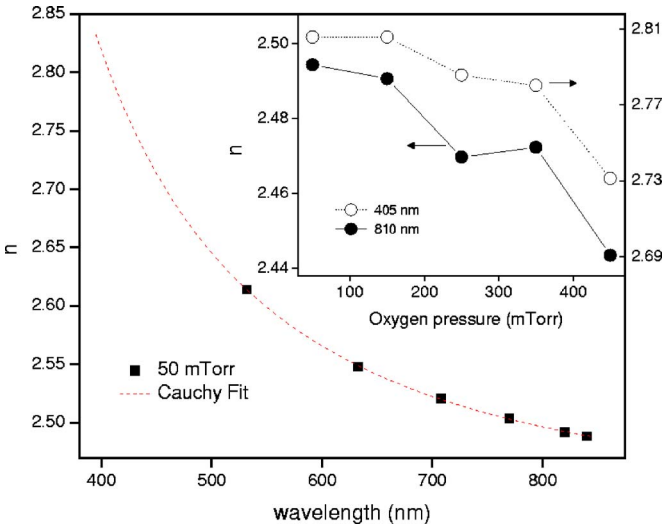

FIG. 2. (Color online) The refraction indices of the PST film deposited under 50 mTorr of oxygen as a function of the wavelength. The inset shows that the refraction indices of PST films decrease as the oxygen pressure increases.

fundamental laser beam is then focused onto the sample (S), which is mounted in a cryostat (CRYO), by a long-focus lens (LL) to achieve a spot size of approximately 139 μm in radius. This results in the incidence peak intensity of about 40 MW/cm^2 at the sample position. The SH signal is measured in the reflection configuration with a fixed incidence angle of 45° for all the SHG measurements. The incidence plane is perpendicular to the [100] direction of PST/MgO as shown in Fig. 4. One long-pass filter (LF) and one bandpass interference filter (BF) are employed to pass the fundamental laser beam immediately before the sample and filter out the SH radiation immediately after the sample, respectively. Two iris diaphragms (IR) are used to confine the collecting angle of the lens (L) and block the reflective beam from the cryostat's window. The SH radiation from the sample is additionally dispersed in a spectrometer and detected by a photomultiplier tube (PMT). The PMT current is then fed into a lock-in amplifier to improve the sensitivity of the device. About 10% of the fundamental laser beam energy is directed

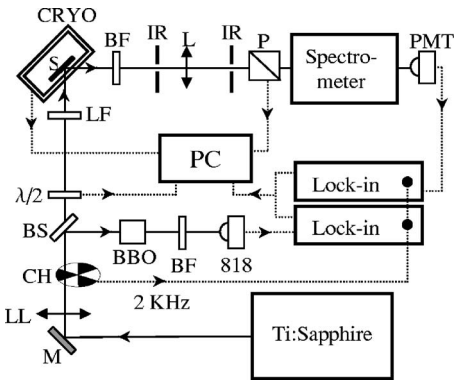

FIG. 3. The schematic of the reflective SHG layout. PMT: photomultiplier tube; 818: Newport 818 semiconductor detector; BBO: BBO nonlinear crystal; CRYO: cryostat; BS: beam splitter; CH: chopper operating at 2 kHz; LF: long-pass filter; BF: bandpass interference filter; λ/2: half-wave plate; P: Glan polarizer; L: lens; LL: long-focus lens; IR: iris diaphragm; M: mirror; PC: computer; S: sample.

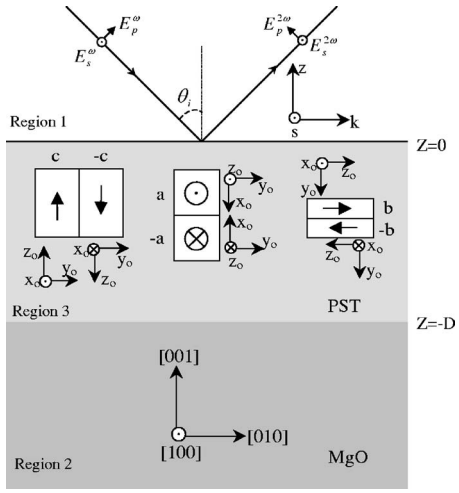

FIG. 4. The schematic of the various domain variants in (001) PST/MgO and the beam geometry for SHG measurements. $\mathbf{x}_0$, $\mathbf{y}_0$, $\mathbf{z}_0$ are the crystallography coordinate axes of the tetragonal PST with $\mathbf{z}_0$ as polar direction. $\mathbf{s}$, $\mathbf{k}$, $\mathbf{z}$ are the beam coordinate axes with $\mathbf{s}$ perpendicular to the incidence plane. D is the film's thickness. θ_i is the incidence angle. Region 1: vacuum; region 2: MgO substrate; region 3: PST film.

through the reference arm containing a nonlinear BBO crystal. The SH radiation from the BBO crystal passes through the same bandpass interference filter and is detected by the Newport 818 large-area semiconductor detector and its current is fed into another lock-in amplifier. The SH radiation from the BBO crystal can be used for providing a reference to remove laser intensity fluctuations. An additional Glan polarizer (P) and a half-wave plate (λ/2) are mounted on the rotating stepper motors to adjust and analyze the polarization directions of the incidence laser beam and the generated SH radiation, respectively. A computer program was written to control the stepper motors and cryostat and to read the outputs from the two lock-in amplifiers. The SH intensities versus the polarization angle or versus the temperature can be obtained.

B. Theoretical consideration

Following Sipe and Sipe *et al.*,[7,8] as shown in Fig. 4, the complex amplitudes of the p- and s-polarized SH fields in the vacuum (region 1) reflected by a nonlinear film with a thickness of D (region 3) deposited on a linear substrate (region 2) are given by

$$E_p^{2\omega} = 2\pi i\tilde{\Omega}^2 W^{-1} T_{31}^{p}\left[\int_{-D}^{0} \exp(-iWz')\hat{\mathbf{P}}_+ \cdot \mathbf{P}^{2\omega}(z')dz' + r_{32}^{s}\exp(2iWD)\int_{-D}^{0}\exp(iWz')\hat{\mathbf{P}}_- \cdot \mathbf{P}^{2\omega}(z')dz'\right], \tag{2a}$$

$$E_s^{2\omega} = 2\pi i\tilde{\Omega}^2 W^{-1} T_{31}^{s}\left[\int_{-D}^{0} \exp(-iWz')\hat{\mathbf{s}} \cdot \mathbf{P}^{2\omega}(z')dz' + r_{32}^{s}\exp(2iWD)\int_{-D}^{0}\exp(iWz')\hat{\mathbf{s}} \cdot \mathbf{P}^{2\omega}(z')dz'\right], \tag{2b}$$

with the notations defined as

$$T_{31}^{(s,p)} = \frac{t_{31}^{(s,p)}}{1 - r_{32}^{(s,p)} r_{31}^{(s,p)} \exp(2iWD)}, \tag{3a}$$

$$W = (\tilde{\Omega}^2 N^2 - K^2)^{1/2}, \quad K = \tilde{\Omega} \sin\theta_i, \quad \tilde{\Omega} = \frac{2\omega}{c}, \tag{3b}$$

$$\hat{\mathbf{P}}_{\pm} = F_s \hat{\mathbf{z}} \mp F_c \hat{\mathbf{k}}, \tag{3c}$$

$$F_s = K/(N\tilde{\Omega}), \quad F_c = W/(N\tilde{\Omega}). \tag{3d}$$

Here, N is the refraction index of the nonlinear film at the SH frequency; $r_{32}^{(s,p)}$, $r_{31}^{(s,p)}$, and $t_{31}^{(s,p)}$ are the Fresnel reflection [$r_{32}^{(s,p)}$ and $r_{31}^{(s,p)}$] and transmission [$t_{31}^{(s,p)}$] coefficients for the s-polarized (superscript s) or p-polarized (superscript p) SH waves incident from the film to the substrate (subscript 32) or vacuum (subscript 31). $\hat{\mathbf{s}}$, $\hat{\mathbf{k}}$, and $\hat{\mathbf{z}}$ are unit vectors along three beam coordinate axes with the incidence plane defined as $(\hat{\mathbf{k}}, \hat{\mathbf{z}})$ shown in Fig. 4; θ_i is the incidence angle of the fundamental beam from the vacuum; $\mathbf{P}^{2\omega}(z)$ is the z-dependent component of the nonlinear polarization. Note that the first term in the bracket on the right-hand side of Eq. (2) describes the contribution to the SH field originating from the upward wave irradiated by the nonlinear polarization, while the second term in the bracket describes the contribution from the downward wave irradiated by the polarization via the reflection [$r_{32}^{(s,p)}$] at the interface between the film and substrate. The effects of the multiple reflections in the film are taken into account in the Fresnel factor $T_{31}^{(s,p)}$. In our case of the small reflectance [$r_{32}^{(s,p)} \ll 1$] at the interface of the ferroelectric PST film and the dielectric MgO substrate, the second term may be omitted compared to the first term. By the same argument, only the nonlinear polarization caused by the downward fundamental beam in the film is considered. Therefore, assuming the z-dependent component of the incident fundamental field has the following form in vacuum:

$$\mathbf{E}^{\omega}(z) = \mathbf{E}^{\omega} \exp(-iw_0 z), \tag{4}$$

we obtain the nonlinear polarization in the film as

$$\mathbf{P}^{2\omega}(z) = \mathbf{P}^{2\omega} \exp(-2iwz), \tag{5}$$

where

$$\mathbf{P}^{2\omega} = \begin{pmatrix} P_s^{2\omega} \\ P_k^{2\omega} \\ P_z^{2\omega} \end{pmatrix} = [d_{ij}] \times \begin{pmatrix} t_s^2 (E_s^{\omega})^2 \\ (f_c t_p)^2 (E_p^{\omega})^2 \\ (f_s t_p)^2 (E_p^{\omega})^2 \\ 2 f_s f_c t_p^2 (E_p^{\omega})^2 \\ 2 f_s t_s t_p E_s^{\omega} E_p^{\omega} \\ 2 f_c t_s t_p E_s^{\omega} E_p^{\omega} \end{pmatrix}, \tag{6a}$$

$$E_s^{\omega} = -E^{\omega} \cos\varphi, \quad E_p^{\omega} = E^{\omega} \sin\varphi, \tag{6b}$$

$$w_0 = \tfrac{1}{2}(\tilde{\Omega}^2 - K^2)^{1/2}, \quad w = \tfrac{1}{2}(n^2\tilde{\Omega}^2 - K^2)^{1/2}, \tag{6c}$$

$$f_s = \frac{K}{n\tilde{\Omega}}, \quad f_c = \frac{2w}{n\tilde{\Omega}}, \tag{6d}$$

where n is the refraction index of the nonlinear film at the fundamental frequency, $[d_{ij}]$ is the matrix form of the nonlinear susceptibility tensor χ_{ijk}, φ is the polarization angle of the incident fundamental beam (φ=90° or 270° for p polarization and φ=0° or 180° for s polarization), and $t_{(s,p)}$ are the Fresnel transmission coefficients for s-polarized (subscript s) or p-polarized (subscript p) fundamental beam incident from vacuum to the film. With these assumptions we substitute Eq. (5) into Eq. (2) and calculate only the first term in the bracket of Eq. (2). The reflected SH fields have the following complex amplitudes:

$$E_p^{2\omega} = -2\pi\tilde{\Omega}^2 W^{-1} T_{31}^{p} [1 - \exp(iD/L_{\text{eff}})] L_{\text{eff}} \hat{\mathbf{P}}_{+} \cdot \mathbf{P}^{2\omega} = S_p \hat{\mathbf{P}}_{+} \cdot \mathbf{P}^{2\omega}, \tag{7a}$$

$$E_s^{2\omega} = -2\pi\tilde{\Omega}^2 W^{-1} T_{31}^{s} [1 - \exp(iD/L_{\text{eff}})] L_{\text{eff}} \hat{\mathbf{s}} \cdot \mathbf{P}^{2\omega} = S_s \hat{\mathbf{s}} \cdot \mathbf{P}^{2\omega}. \tag{7b}$$

Here, $L_{\text{eff}} = 1/(W+2w)$ is the coherent length in the reflection geometry. For simplicity, we may ignore the birefringence of the various ferroelectric domains, and assume that S_p and S_s are independent on the orientation of the domains. Therefore, S_p and S_s may be taken as the scaling factors when we fit the experimental data.

Perovskite $(Pb,Sr)TiO_3$ in its ferroelectric state has a symmetry of point group $4mm$. The third-rank nonlinear susceptibility tensor χ_{ijk} has three independent components and can be written as the following matrix $[d_{ij}]$ with respect to the crystallography coordinate axes $(\hat{\mathbf{x}}_0, \hat{\mathbf{y}}_0, \hat{\mathbf{z}}_0)$:

$$[d_{ij}] = \begin{bmatrix} 0 & 0 & 0 & 0 & \alpha & 0 \\ 0 & 0 & 0 & \alpha & 0 & 0 \\ \beta & \beta & \gamma & 0 & 0 & 0 \end{bmatrix}. \tag{8}$$

Generally, six domain variants exist in the tetragonal $(Pb,Sr)TiO_3$ films deposited on the cubic (001) MgO substrates. Their polar directions may be parallel or antiparallel to three crystallography axes of the MgO substrates, i.e, the [100] axis ($\pm a$ domain), [010] axis ($\pm b$ domain), and [001] axis ($\pm c$ domain) as shown in Fig. 4. The susceptibility tensors with respect to the beam coordinate axes $(\hat{\mathbf{s}}, \hat{\mathbf{k}}, \hat{\mathbf{z}})$ for various domains can be derived from their representation in the crystallography coordinate axes $(\hat{\mathbf{x}}_0, \hat{\mathbf{y}}_0, \hat{\mathbf{z}}_0)$ via the tensor transformation $\chi'_{ijk} = \alpha_{il}\alpha_{jm}\alpha_{kn}\chi_{lmn}$, where $[\alpha_{ij}]$ is the corresponding coordinate transformation matrix. The susceptibility tensors of the various domains with respect to the beam coordinate axes have been calculated and listed in Table I. Substituting the susceptibility tensors into Eq. (6a) and combining Eq. (7), the SH fields generated by various domains can be calculated and the final results are also listed in Table I.

As expected, the SH fields generated by the positive and negative domains cancel each other. Using the similar technique as Gopalan and Raj,[4] Barad *et al.*,[5] and Mishina *et al.*,[3] we denote the differences of the fractions of positive and

TABLE I. The nonlinear susceptibilities $\chi_{ijk}(d_{ij})$ with respect to the beam coordinate axes and the reflected SH fields $E^{2\omega}_{(s,p)}$ generated by the various domain variants [the negative domain variants have the same absolute value and the opposite sign of χ_{ijk} (d_{ij}) and $E^{2\omega}_{(s,p)}$ as the corresponding positive domain variants] shown schematically in Fig. 4.

Domain variant	*c* domain	*a* domain	*b* domain
$d_{ij}(\chi_{ijk})$	$d^c_{15}=d^c_{24}=\alpha$, $d^c_{31}=d^c_{32}=\beta$, $d^c_{33}=\gamma$	$d^a_{12}=d^a_{13}=\beta$, $d^a_{26}=d^a_{35}=\alpha$, $d^a_{11}=\gamma$	$d^b_{16}=d^b_{34}=\alpha$, $d^b_{21}=d^b_{23}=\beta$, $d^b_{22}=\gamma$
$E^{2\omega}_s/S_s(E^\omega)^2$	$-2\alpha f_s t_s t_p \cdot \cos\varphi \sin\varphi$	$\beta t_p^2 \sin\varphi^2 + \gamma t_s^2 \cos\varphi^2$	$-2\alpha f_c t_s t_p \cdot \cos\varphi \sin\varphi$
$E^{2\omega}_p/S_p(E^\omega)^2$	$(\beta f_c^2 F_s + \gamma f_s^2 F_s - 2\alpha f_c f_s F_c)\, t_p^2 \sin\varphi^2 + \beta F_s t_s^2 \cos\varphi^2$	$-2\alpha(f_s F_s - f_c F_c)\cdot t_s t_p \cos\varphi \sin\varphi$	$(2\alpha f_c f_s F_s - \beta f_s^2 F_c - \gamma f_c^2 F_c)\, t_p^2 \sin\varphi^2 - \beta F_c t_s^2 \cos\varphi^2$

negative domains as $\Delta F_a = F_a - F_{-a}$, $\Delta F_b = F_b - F_{-b}$, and $\Delta F_c = F_c - F_{-c}$, where F_i is the fraction of the corresponding i domain. The total reflected coherent SH intensity can be written as

$$I^{2\omega}_{(s,p)} = |\Delta F_a E^{2\omega,a}_{(s,p)} + \Delta F_b E^{2\omega,b}_{(s,p)} + \Delta F_c E^{2\omega,c}_{(s,p)}|^2. \tag{9}$$

The incidence polarization angle (φ) dependence of the above SH intensity can be fitted via the following function:

$$I^{2\omega}_{(s,p)} = [a_{(s,p)} \cos\varphi^2 + b_{(s,p)} \sin\varphi^2 + c_{(s,p)} \cos\varphi \sin\varphi]^2 + d_{(s,p)}, \tag{10}$$

where $a_{(s,p)}$, $b_{(s,p)}$, $c_{(s,p)}$, and $d_{(s,p)}$ are the fitting parameters. $d_{(s,p)}$ is artificially added to simulate the system's background. Substituting the formula for SH fields generated by various domains (listed in Table I) into Eq. (9) and comparing the coefficients of Eqs. (9) and (10), we obtain the relations between the fitting parameters and the physical quantities as follows:

$$\frac{\gamma}{\beta} = \left(\frac{a_s}{b_s}\right)\left(\frac{t_p}{t_s}\right)^2, \tag{11}$$

$$\frac{\Delta F_c}{\Delta F_a} = \frac{t_p}{(f_s F_c + f_c F_s) t_s} \times \left[2\left(\frac{a_p}{c_p}\right)\left(\frac{\alpha}{\beta}\right)(f_c F_c - f_s F_s) f_c - \frac{1}{2}\left(\frac{c_s}{b_s}\right)\left(\frac{\beta}{\alpha}\right) F_c\right], \tag{12}$$

$$\frac{\Delta F_b}{\Delta F_a} = \frac{t_p}{(f_s F_c + f_c F_s) t_s} \times \left[-2\left(\frac{a_p}{c_p}\right)\left(\frac{\alpha}{\beta}\right)(f_c F_c - f_s F_s) f_s - \frac{1}{2}\left(\frac{c_s}{b_s}\right) \times \left(\frac{\beta}{\alpha}\right) F_s\right], \tag{13}$$

$$\frac{\Delta F_c}{\Delta F_b} = \frac{\Delta F_c / \Delta F_a}{\Delta F_b / \Delta F_a}, \tag{14}$$

where the ratio β/α or α/β of the nonlinear susceptibilities is obtained by solving the following third-order polynomial equation:

$$\left(\frac{\beta}{\alpha}\right)^3 + a\left(\frac{\beta}{\alpha}\right)^2 + b\left(\frac{\beta}{\alpha}\right) + c = 0. \tag{15}$$

The coefficients in Eq. (14) are given by

$$a = -\frac{f_c f_s (F_c^2 - F_s^2)}{F_c F_s (f_c^2 - f_s^2)} \frac{2}{1 - \gamma/\beta},$$

$$b = \frac{-4(f_c F_c - f_s F_s)\{(a_p b_s / c_p c_s)[(f_s^3 F_c + f_c^3 F_s) + \gamma/\beta f_c f_s (f_c F_c + f_s F_s)] - (b_p b_s / c_p c_s)(f_s F_c + f_c F_s) t_s^2 / t_p^2\}}{F_c F_s (f_c^2 - f_s^2)(1 - \gamma/\beta)}$$

$$c = \frac{f_c f_s (f_c^2 F_c^2 - f_s^2 F_s^2)}{F_c F_s (f_c^2 - f_s^2)} \frac{a_p}{c_p} \frac{b_s}{c_s} \frac{8}{1 - \gamma/\beta}. \tag{16}$$

Equations (11) and (15) can be used to calculate the ratios of the three components of the nonlinear susceptibility tensor while Eqs. (12)–(14) can be used to determine the ratios of the compensated domain fractions. All the Fresnel factors in Eqs. (11)–(16) may be calculated via the Fresnel laws by referring the film's refraction indices measured in Sec. III. $f_{(s,c)}$ and $F_{(s,c)}$ are calculated via Eqs. (3d) and (6d). Note that, generally Eq. (15) has three solutions. We take the positive real solution that is most close to the Kleinman symmetry $(\beta/\alpha \sim 1)$.

C. Experimental results and discussion

The SH fields generated by the films were analyzed by rotating the Glan polarizer at several typical temperatures. The SH intensities generated by all five samples exhibit the similar dependence on the analyzer angle (ϕ). Typically, Figs. 5(a) and 5(b) are the polar plots for the SH intensities as a function of ϕ under the incidence of the *s*- or *p*-polarized fundamental beams, respectively, at the temperatures of 78 K (solid squares) and 300 K (open squares) for the film deposited at the oxygen pressure of 50 mTorr. The

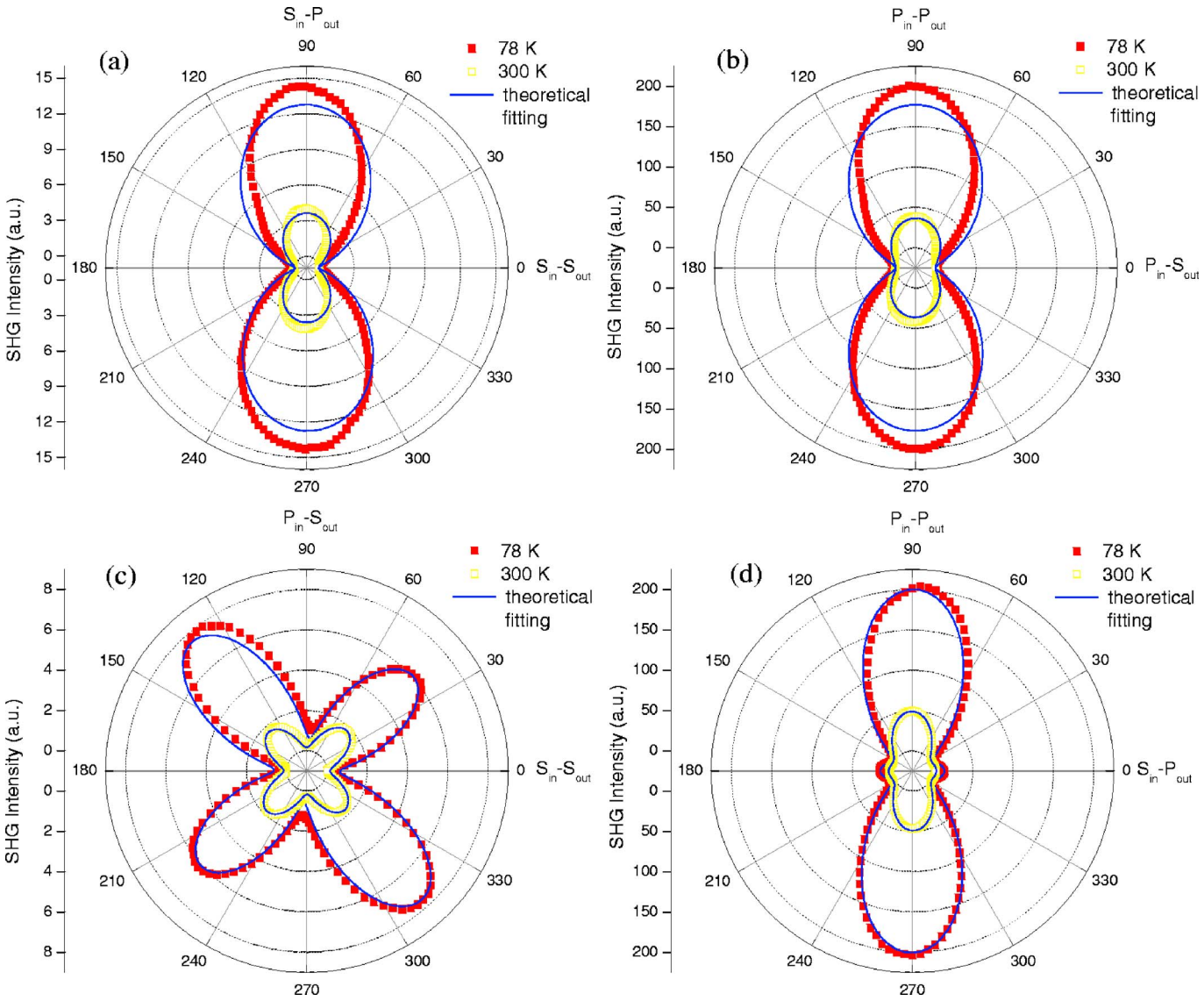

FIG. 5. (Color online) SHG polarization diagrams for the PST film deposited under the oxygen pressure of 50 mTorr. Filled squares correspond to SH intensity measured at 300 K, open squares correspond to SH intensity measured at 78 K, and solid lines correspond to the theoretical fits. [(a) and (b)] Analyzer angle dependence; [(c) and (d)] incidence polarization angle dependence.

experimental data are theoretically fitted (solid lines) by the method of "least squares" via the following equation:[9]

$$I^{2\omega} = A^2 \cos\phi^2 + B^2 \sin\phi^2 - 2AB \cos\phi \sin\phi \cos\Delta, \tag{17}$$

where A and B correspond to the amplitudes of the s- and p-polarized SH fields, Δ is the possible phase difference between them, ϕ=90° or 270° stands for p-polarized SH field, and ϕ=0° or 180° stands for the s-polarized SH field. As shown in Figs. 5(a) and 5(b), the SHG under the incidence of s- or p-polarized fundamental beam shows a strong temperature dependence in intensity and has a similar shape with the zero phase difference (Δ=0) and the dominating p-polarized SH field ($B^2/A^2 \gg 1$).

The intensities of the s- and p-polarized SH radiation as a function of the polarization angle (φ) of the fundamental beam at two typical temperatures (78 and 300 K) for the PST film deposited at 50 mTorr are shown in Figs. 5(c) and 5(d). The shapes of the polar plots are less temperature dependent. The maximal p-polarized SH intensity occurs under the incidence of the p-polarized fundamental beam whereas the maximal s-polarized SH intensity occurs under the incidence of the fundamental beam of a mixed polarization with the polarization angle of about 45°. The experimental data were fitted by the method of least squares via Eq. (10). The ratios of ΔF_i and the ratios of α, β, and γ may be calculated via Eqs. (11)–(16). The final results for the five samples at three typical temperatures (78, 150, and 300 K) are listed in Table II. The changes of $\Delta F_b/\Delta F_a$ are considered as the fluctuation of the compensated in-plane domains because of the equivalence of positive and negative a domains. All samples exhibit much larger compensated fractions of c domains than in-plane domains at all temperatures. It is expected because of the strain induced by the large lattice mismatch between PST and MgO. We found that the ratios of $\Delta F_c/\Delta F_b$ and the ratios of γ/β and α/β were relatively constant, except for some of the abnormal data labeled by star, regardless of the temperature and oxygen pressure. It is very likely that such

TABLE II. The ratios of the components of the nonlinear susceptibility tensor and the ratios of the compensated domain fractions calculated via Eqs. (11)–(16) at three typical temperatures (78, 150, and 300 K) for the epitaxial PST films deposited on (001) MgO substrates under different oxygen pressures.

Oxygen pressure (mTorr)	Temperature (K)	γ/β	β/α	$\lvert\Delta F_b/\Delta F_a\rvert$	$\lvert\Delta F_c/\Delta F_b\rvert$
	78	−0.40	0.30	64.0	3.30
50	150	−0.50	0.29	29.9	3.19
	300	0.87[a]	0.21	36.2	2.25
	78	−0.29	0.35	24.8	2.96
150	150	−0.29	0.36	40.5	3.18
	300	−0.15	0.28	53.5	3.13
	78	−0.33	0.28	1075.9	3.37
250	150	0.99[a]	0.25	26.2	2.52
	300	−0.25	0.33	19.1	3.8
	78	−0.0041[a]	2.37[a]	32.2	3.8
350	150	0.43[a]	0.48	5.9	7.8
	300	−0.0013[a]	0.32	163.6	3.29
	78	0.76[a]	0.29	30.5	1.9
450	150	−0.58	0.52	24.7	4.53
	300	−0.73	0.45	82.9	3.18

[a]Abnormal data.

abnormal data are due to the large fitting errors of least squares (more than 100% parameter errors for these abnormal data). The independent ratio of domain fractions is an indication that the domain redistribution is difficult when the sample is cooled down or the deposition pressure is changed. It is consistent with our knowledge of the large energy required for domain switching.

Figure 6 shows the *p*-polarized SH intensities as a function of temperature in the range of 78–320 K for the five samples deposited under 50–450 mTorr oxygen pressures. The measurements were performed under the incidence of the *p*-polarized fundamental beam. The continuous increase of the SH intensity in a wide temperature range was an obvious feature of "diffuse phase transition" from cubic phase to tetragonal phase in our PST films. The phase transition point (T_m) as indicated by the dashed line was determined to be around 280 K by the dielectric measurement using the interdigital technique. The columnar structures (as shown in the transmission electron microscopy image of Ref. 2) will develop in our PST films with the structural inhomogeneity and the nonuniform substitution of Pb^{2+} by Sr^{2+} in chemistry. Such an inhomogeneity in ferroelectric materials will cause a broadened phase transition. The curves also exhibit small intensity peaks as labeled by the small arrows in Fig. 6. This feature is not well understood to date. It has been observed in a similar ferroelectric film of $(Pb,La)(Zr,Ti)O_3$.[10] It was suggested that it was most likely that some slow relaxation mechanisms such as slowly diffusing charged defects in the film might contribute to such a feature because these peaks were dependent on the cooling rate.[10]

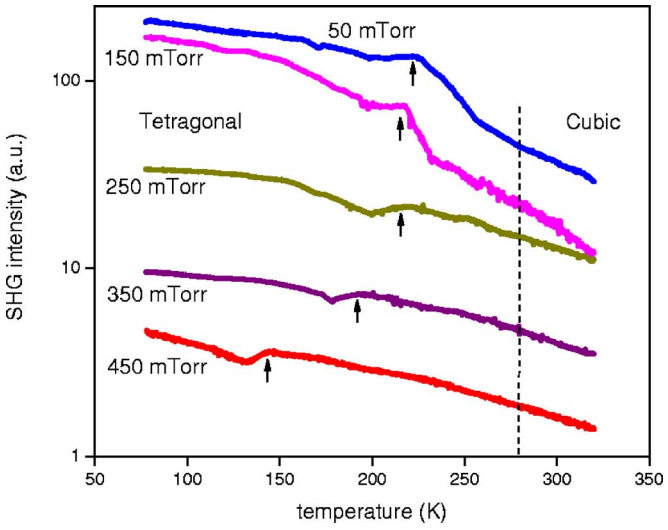

FIG. 6. (Color online) Temperature dependence of the SH intensities for PST films deposited under the oxygen pressures of 50–450 mTorr.

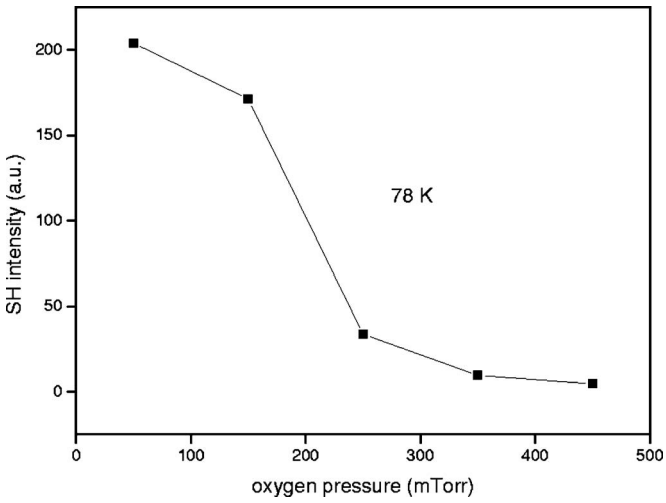

FIG. 7. SH intensities measured at 78 K from the five films deposited under different oxygen pressures.

We found that the SH intensity was strongly dependent on the oxygen pressure as shown in Fig. 7. The SH intensity increases significantly as the oxygen pressure decreases. Substituting the formula for SH fields into Eq. (9) and taking $\varphi=90°$, we obtain

$$I_p^{2\omega}=[(2f_cf_sF_s\alpha/\beta-f_c^2F_c\gamma/\beta-f_s^2F_c)\Delta F_b/\Delta F_c - (2f_cf_sF_c\alpha/\beta-f_s^2F_s\gamma/\beta-f_c^2F_s)]t_p^2\Delta F_c\beta\propto\Delta F_c\beta. \quad (18)$$

As we have calculated, the ratios of $\Delta F_c/\Delta F_b$ and the ratios of α/β and γ/β are relatively constant for different films. The small variation of the linear refraction indices for different films may also be ignored. Assuming the same values of the compensated domain fractions ΔF_c, it indicates that the nonlinear susceptibility of the PST film becomes larger as the oxygen pressure decreases. It may be attributed to the increased density of oxygen vacancies in the films. Generally, a higher density of oxygen vacancies will incur a larger distortion of the PST unit cell and improve its nonlinearity. The absolute value of the nonlinear susceptibility of the PST film (250 mTorr) was found to be comparable to the value of the similar BST ($Ba_{0.6}Sr_{0.4}TiO_3$) film grown on the (001) MgO

substrate under the same condition by comparing their SH intensities and polarization diagrams. The BST film has a large nonlinear susceptibility claimed by another group.[11] It indicates that the PST has the potential applications in the nonlinear optical devices.

V. CONCLUSIONS

In conclusion, SHG were measured at different temperatures for five PST films epitaxially deposited on (001) MgO substrates under different oxygen pressures. We formulated the procedures to measure the ratios of the compensated domain fractions and the components of the nonlinear susceptibility tensor under a single non-normal incidence in reflection geometry. These ratios are independent on the oxygen pressure and the measuring temperature. It indicates that the domain redistribution is difficult when the samples are cooled down or the deposition oxygen pressure is changed. The films also exhibit a continuous increase of the SH intensity in a wide temperature range as the samples were cooled down due to their inhomogeneity in both structure and chemistry. The SH intensity increases significantly as the oxygen pressure decreases, which is attributed to the increased density of oxygen vacancies in the films.

ACKNOWLEDGMENTS

The authors acknowledge the funding supports from the Army Research Office and NSF.

[1] S. W. Liu *et al.*, Appl. Phys. Lett. **85**, 3202 (2004).
[2] S. W. Liu *et al.*, Appl. Phys. Lett. **87**, 142905 (2005).
[3] E. D. Mishina, N. E. Sherstyuk, D. R. Barskiy, A. S. Sigov, Yu. I. Golovko, V. M. Mukhorotov, M. De Santo, and Th. Rasing, J. Appl. Phys. **93**, 6216 (2003).
[4] V. Gopalan and R. Raj, Appl. Phys. Lett. **68**, 1323 (1996).
[5] Y. Barad, J. Lettieri, C. D. Theis, D. G. Schlom, and V. Gopalan, J. Appl. Phys. **89**, 1387 (2001).
[6] The values for a typical peroskite $SrTiO_3$ were estimated from "T. Toyoda and M. Yabe, J. Phys. D **16**, L251 (1983);" The values for MgO were estimated from "R. E. Stephens and I. H. Malitson, J. Res. Natl. Bur. Stand. **49**, 249 (1952)."
[7] J. E. Sipe, J. Opt. Soc. Am. B **4**, 481 (1987).
[8] J. E. Sipe, D. J. Moss, and H. M. van Driel, Phys. Rev. B **35**, 1129 (1986).
[9] E. D. Mishina, T. V. Misuryaev, N. E. Sherstyuk, V. V. Lemanov, A. I. Morozov, A. S. Sigov, and Th. Rasing, Phys. Rev. Lett. **85**, 3664 (2000).
[10] M. Pavel, I. Rychetsky, and J. Petzelt, J. Appl. Phys. **89**, 5036 (2001).
[11] U. C. Oh, J. Ma, G. K. L. Wong, J. B. Ketterson, and J. H. Je, Appl. Phys. Lett. **76**, 1461 (2000).